

X-ray diffuse scattering study on charge-localized states of $\text{Pr}_{1-x}\text{Ca}_x\text{MnO}_3$ ($x=0.35,0.4,0.5$)

S. Shimomura,¹ T. Tonegawa,¹ K. Tajima,¹ N. Wakabayashi,¹ N. Ikeda,² T. Shobu,³ Y. Noda,⁴ Y. Tomioka,⁵ and Y. Tokura^{5,6}

¹*Department of Physics, Faculty of Science and Technology, Keio University, 3-14-1 Hiyoshi, Kohoku-ku, Yokohama 223-8522, Japan*

²*Japan Synchrotron Research Institute, SPring-8, Mikazuki, Sayo-gun, Hyogo 679-5198, Japan*

³*Department of Physics, Chiba University, 1-33 Yayoi, Inage, Chiba 263-8522, Japan*

⁴*Research Institute for Scientific Measurements, Tohoku University, 2-1-1 Katahira, Aoba-ku, Sendai 980-8577, Japan*

⁵*Joint Research Center for Atom Technology (JRCAT), Tsukuba 305-8562, Japan*

⁶*Department of Applied Physics, University of Tokyo, Tokyo 113-8656, Japan*

(Received 22 February 2000)

X-ray scattering measurements on $\text{Pr}_{1-x}\text{Ca}_x\text{MnO}_3$ ($x=0.35,0.40,0.50$) have revealed the existence of diffuse scattering above the charge and orbital ordering transition temperature (T_{CO}). The diffuse scattering has local intensity maxima at incommensurate positions $(0, \pm \zeta, 0)$. With decreasing temperature, ζ increases from about 0.4, and it discontinuously changes to 0.5 at T_{CO} . Characteristic patterns of diffuse intensity distributions can be qualitatively interpreted by calculations based on distortion fields associated with the Jahn-Teller effect. The observed patterns are similar to those observed above the ferromagnetic insulator-metal transition temperature in $(\text{Nd}_{0.125}\text{Sm}_{0.875})_{0.52}\text{Sr}_{0.48}\text{MnO}_3$ reported previously.

Manganese oxides with distorted perovskite structures, $A_{1-x}B_x\text{MnO}_3$ (A is a trivalent rare-earth ion, and B is a divalent alkaline-earth ion), are interesting systems because of their colossal magnetoresistance and charge ordering phenomena. It has been pointed out that strong electron-lattice coupling is important to understand these phenomena.¹ The nature of the local lattice distortion due to the localization of charges has been one of major subjects of experimental and theoretical studies. Recently, local lattice distortion due to the localization of carriers on Mn sites has been reported to exist in the paramagnetic insulating phase and to disappear in the ferromagnetic metallic phase.^{2,3} Significant correlation between charges dressed with local lattice distortion may be present in these compounds, but details are still unclear.

In contrast to the compounds showing the ferromagnetic insulator-to-metal transition, $\text{Pr}_{1-x}\text{Ca}_x\text{MnO}_3$ with $0.3 \leq x \leq 0.5$ exhibits the charge ordering transition and the antiferromagnetic transition.⁴⁻⁸ Below the charge-ordering transition temperature (T_{CO}), the Mn^{3+} and Mn^{4+} ions are ordered alternatively in the a - b plane. The cooperative Jahn-Teller (JT) transition associated with the orbital ordering simultaneously occurs at T_{CO} . This ordering results in the doubling of the crystallographic unit cell. When an external magnetic field is applied, the charge-ordered insulating phase is transformed into the ferromagnetic metallic phase. Although the charge and orbital ordering transition coincides with an antiferromagnetic transition in some manganites, $\text{Pr}_{1-x}\text{Ca}_x\text{MnO}_3$ has the charge ordering transition temperature different from the Néel temperature.⁴ Thus $\text{Pr}_{1-x}\text{Ca}_x\text{MnO}_3$ is a suitable system to investigate the effect of the charge localization on crystal lattices without complication of magnetoelastic effect. The purpose of the present x-ray diffuse scattering measurements is to study local lattice distortion due to the charge localization. The development of the correlation between distortion fields can be regarded as a precursor phenomenon of the charge and orbital ordering transition. The results obtained in this study are compared with those obtained previously above the ferro-

magnetic insulator-to-metal transition temperature in $(\text{Nd}_{0.125}\text{Sm}_{0.875})_{0.52}\text{Sr}_{0.48}\text{MnO}_3$.²

Single crystals of $\text{Pr}_{1-x}\text{Ca}_x\text{MnO}_3$ ($x=0.35,0.40,0.50$) were grown by the floating zone method. The crystal structure⁵ is orthorhombic with the pseudocubic relation among the lattice parameters specified by $a \approx b \approx c/\sqrt{2} \approx \sqrt{2}a_c$, where a_c is the lattice parameter of the cubic-perovskite lattice. As-grown crystals were composed of pseudocubic domains. Crystals were cut so that one dominant fraction of volume consists of the suitable domain. The sample sizes were approximately $2 \times 2 \times 0.5$ mm³. X-ray scattering measurements were performed using a two-axis diffractometer with Mo- $K\alpha$ radiation (50 kV, 150 mA) monochromatized by the 002 reflection of a pyrolytic graphite crystal. To eliminate unwanted scattering, a pyrolytic graphite crystal was also used as an analyzer crystal. The sample was mounted inside a closed-cycle He refrigerator. The temperature dependence of the diffuse scattering was measured along the [010] direction through the (10,0,0) point for the $x=0.4$ and 0.5 crystals, and through the (8,0,0) point for the $x=0.35$ crystal. In addition, the intensity distributions around (8,0,0) and (8,8,0) were measured in the ($hk0$) reciprocal plane above T_{CO} . The intensity distribution around (10,4,0) in the $x=0.4$ crystal was also measured at 300 K by using synchrotron radiation. This measurement was performed on the BL02B1 at the SPring-8. The x-ray energy was 29.94 keV.

Figure 1 shows examples of the diffuse scattering profiles along the [010] direction through the (10,0,0) point in $\text{Pr}_{0.5}\text{Ca}_{0.5}\text{MnO}_3$. The diffuse scattering is clearly seen at 300 K. The profile has local intensity maxima at the positions of $(10, \pm \zeta, 0)$ with $\zeta \approx 0.4$. With decreasing temperature, the local maxima grow and their positions shift towards $\zeta=0.5$. Intense reflections as narrow as an experimental resolution were observed at the commensurate positions of $\zeta=0.5$ below $T_{\text{CO}}=235$ K. The diffuse peaks observed above T_{CO} probably arise from the development of the short-range correlation associated with the formation of the charge and orbital orderings.

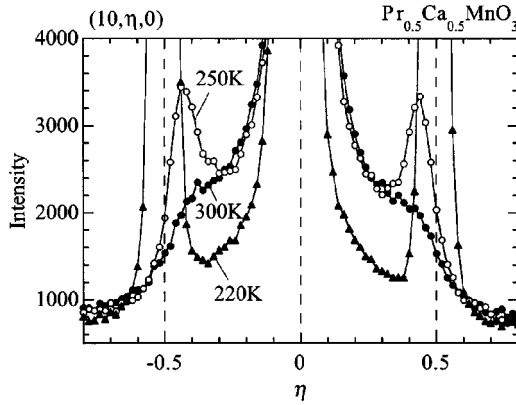


FIG. 1. Temperature dependence of diffuse scattering profiles along the $[100]$ direction through $(10,0,0)$ in $\text{Pr}_{0.5}\text{Ca}_{0.5}\text{MnO}_3$. Local intensity maxima exist around $(10, \pm\zeta, 0)$ with $\zeta \approx 0.40$ at 300 K and with $\zeta \approx 0.43$ at 250 K. Below the charge-ordering transition temperature ($T_{\text{CO}} = 235$ K), ζ becomes 0.5.

The temperature dependences of the peak position, intensity, and widths are shown in Figs. 2(a)–(c), respectively. The modulation wave number, corresponding to the peak position, increases monotonically with decreasing temperature. It discontinuously increases to the commensurate value of $0.5b^*$ at T_{CO} . The peak intensity increases with decreasing temperature and discontinuously changes at T_{CO} . The widths along the $[100]$ and $[010]$ directions decrease with decreasing temperature, and they discontinuously decrease to respective experimental resolutions at T_{CO} . These results show that the correlation characterized by the incommensurate modulation develops with decreasing temperature, and the long-range order of the commensurate lattice modulation is established below T_{CO} .

Similar peaks were also observed in the $x=0.35$ and 0.4 crystals. The temperature dependences of the wave numbers for $x=0.35, 0.4, 0.5$ are summarized in Fig. 3. The incommensurate wave number increases with decreasing temperature in the $x=0.35$ and 0.4 crystals as well as $x=0.5$. The modulation wave numbers have larger values for lower x at any given temperature above T_{CO} . The discontinuous change in the wave number at T_{CO} becomes smaller for smaller x .

It should be noted that the wave vector is incommensurate above T_{CO} even in the half doped crystal ($x=0.5$) having the stoichiometric charge concentration corresponding to the charge-ordered state. In contrast, below T_{CO} the wave number becomes to the commensurate value of 0.5 not only in the $x=0.5$ crystal but also in the $x=0.35$ and 0.40 crystals.

As seen in Fig. 1, a component of the diffuse scattering centered at the $(10,0,0)$ point seems to exist above T_{CO} . The diffuse intensity within $|\zeta| < 0.2$ slightly decreases with decreasing temperature, and it seems to vanish below T_{CO} . The intensity distributions in reciprocal space show characteristic patterns depending on the reciprocal lattice points. Figure 4(a) shows the contour plot of the intensity distribution in the $(hk0)$ reciprocal lattice plane around $(8,0,0)$ observed at 250 K in the $x=0.5$ crystal. In addition to the peaks around $(8, \pm 0.45, 0)$, the intensity distribution extends along the $[010]$ direction. In contrast, a butterfly-shaped pattern extending nearly along the $[100]$ and $[010]$ directions was observed

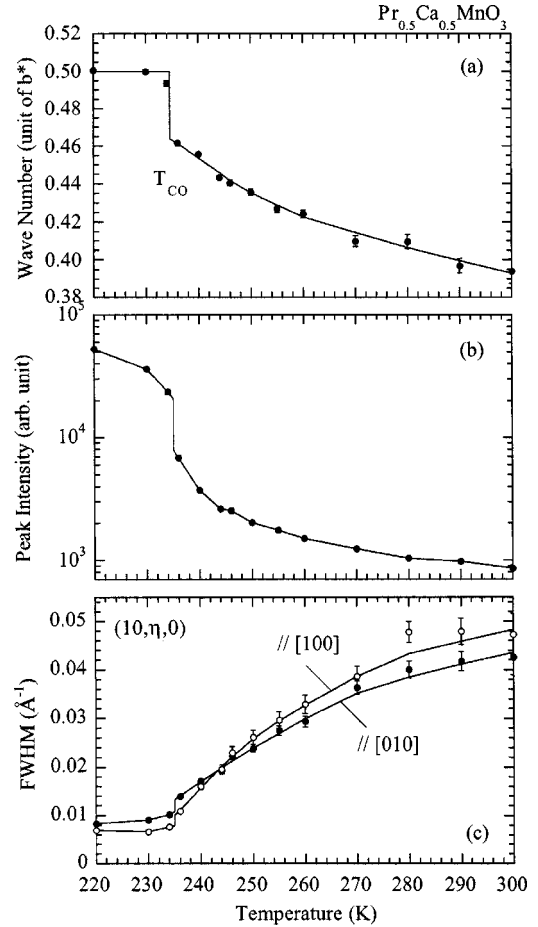


FIG. 2. Temperature dependences of the (a) wave number, (b) intensity, and (c) widths along the $[100]$ and $[010]$ directions in $\text{Pr}_{0.5}\text{Ca}_{0.5}\text{MnO}_3$. The modulation wave number increases with decreasing temperature, and it discontinuously changes to 0.5 at T_{CO} when the long-range charge order is established.

around $(8,8,0)$ at 300 K as shown in Fig. 4(b). The peaks characterized by the incommensurate modulation are not evident at 300 K ($T_{\text{CO}} + 65$ K), but well developed at 250 K [Fig. 4(a)]. In Fig. 4(a), the intensity distribution extending along the $[100]$ direction and passing through the $(8,0,0)$ point is due to contamination by radiation having wave-

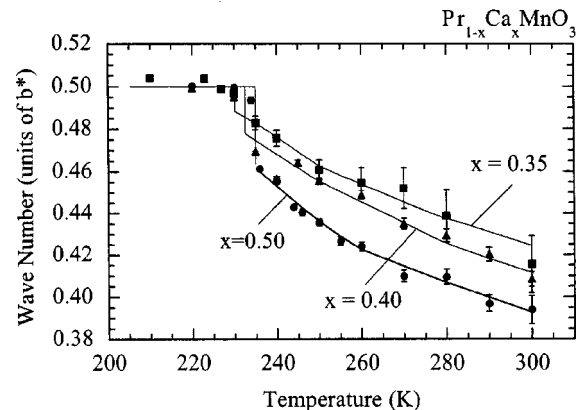


FIG. 3. Temperature dependences of the modulation wave number in $\text{Pr}_{1-x}\text{Ca}_x\text{MnO}_3$ with $x=0.35, 0.4, 0.5$. Solid lines are guides for the eye. All the data were collected for decreasing temperature.

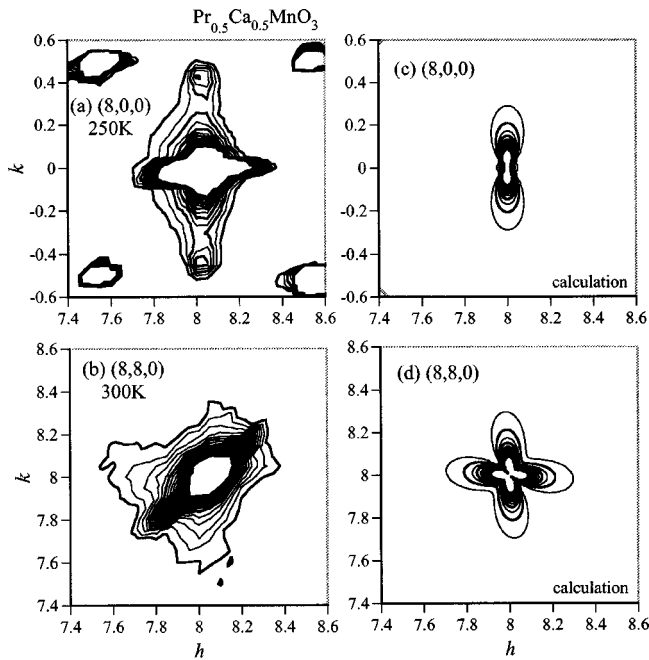


FIG. 4. Contour plots of diffuse scattering intensities observed around (a) (8,0,0) and (b) (8,8,0) in $\text{Pr}_{0.5}\text{Ca}_{0.5}\text{MnO}_3$. The intensity distribution around (8,0,0) extends along the [010] direction. A butterfly-shaped pattern extending along the [100] and [010] directions is seen around (8,8,0). The streaks passing through the reciprocal lattice points and extending toward the origin of the reciprocal lattice are due to contamination (see text). Calculated patterns of the diffuse intensity based on the local lattice distortion due to the Jahn-Teller effect are shown in (c) (8,0,0) and (d) (8,8,0).

lengths slightly different from that of the $K\alpha$ radiation. A similar contamination extending along the [110] direction is also seen in Fig. 4(b). Fundamental Bragg peaks around $(h \pm 0.5, k \pm 0.5, 0)$ and $(h \pm 0.5, k \mp 0.5, 0)$ arise from domain structures. For example, the one centered around (8.5,0.5,0) corresponds to (4,4,9) of a different domain.

Similar patterns of diffuse scattering distribution were observed for the $x=0.35$ and $x=0.4$ crystals. We also collected intensity data around (10,4,0) in the $x=0.4$ crystal using synchrotron radiation. Figure 5(a) shows a contour plot of the intensity distribution observed at 300 K. The contamination mentioned above was not detected because of high-energy resolution of the x rays. In addition to the diffuse intensity distribution extending along the [010] direction, small extension nearly along the [100] direction is seen.

We calculated the diffuse intensity in the same manner as previously reported.² The local lattice distortion is postulated to arise from the JT distortion of a Mn^{3+}O_6 octahedron having two long Mn-O bonds and four short Mn-O bonds. This distortion induces a distortion field in the surrounding lattice. For the simplicity of the calculation, we assume that Mn^{3+}O_6 octahedra are independent of each other and that the surrounding lattice is an elastic medium. The scattering intensity can be calculated as the Huang scattering intensity.^{9,10} As shown in Figs. 4(c) and (d), the calculated intensity distributions around (8,0,0) and (8,8,0) show a two-lobes pattern and a butterfly-shaped pattern, respectively. The observed pattern around (10,4,0) is consistent with the corresponding calculation shown in Fig. 5(b). Over-

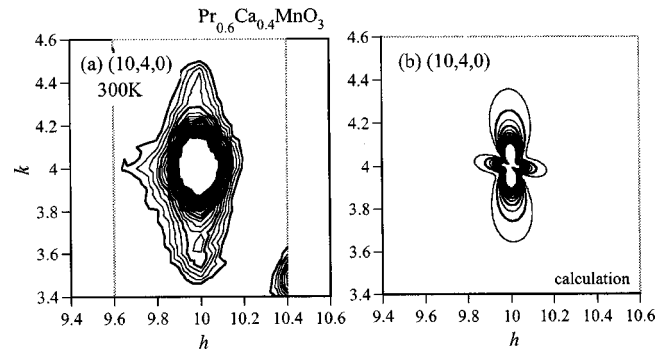


FIG. 5. (a) Contour plot of diffuse scattering intensities around (10,4,0) in $\text{Pr}_{0.6}\text{Ca}_{0.4}\text{MnO}_3$ measured by using synchrotron radiation. (b) Intensity distribution calculated in the same manner as those shown in Fig. 4.

all agreement between the calculation and the observation is satisfactory, indicating that the diffuse intensity is attributable to the local lattice distortion associated with the JT distortion.

In contrast to the calculations, the observed intensity distribution around (8,8,0) and (10,4,0) are asymmetric about the respective reciprocal points as shown in Figs. 4(b) and 5(a). In addition, the diffuse scattering has local intensity maxima at the incommensurate positions. These features probably arise from the development of the correlation between the distortion fields. The correlation is probably related to the fluctuations of charge and orbital orderings. According to resonant x-ray scattering study,⁸ the commensurate charge-order fluctuations are highly correlated above T_{CO} . The incommensurate lattice modulation may primarily arise from the fluctuation of the orbital ordering which participate in the cooperative JT ordering. Just above T_{CO} , discommensurations,¹¹ i.e., antiphase domain boundaries between two commensurate orbital-ordered regions, seem to exist and to be periodically arranged.

It should be pointed out that similar patterns of the intensity distributions² have been also observed in a pseudocubic compound of $(\text{Nd}_{0.125}\text{Sm}_{0.875})_{0.52}\text{Sr}_{0.48}\text{MnO}_3$ exhibiting the insulator-metal transition concomitant with the ferromagnetic transition.¹² The diffuse intensity increases with decreasing temperature towards the ferromagnetic transition temperature (T_{C}) and vanishes abruptly below T_{C} . Small local maxima around $(\pm \zeta, 0, 0)$ and $(0, \pm \zeta, 0)$ with $\zeta \approx 0.3-0.35$ were also observed. These results suggest that the correlation between distortion fields associated with the JT distortion exist above T_{C} in $(\text{Nd}_{0.125}\text{Sm}_{0.875})_{0.52}\text{Sr}_{0.48}\text{MnO}_3$ as well as above T_{CO} in $\text{Pr}_{1-x}\text{Ca}_x\text{MnO}_3$. The short-range charge order develops into the long-range order in $\text{Pr}_{1-x}\text{Ca}_x\text{MnO}_3$. By contrast, the ferromagnetic metallic phase is stabilized in $(\text{Nd}_{0.125}\text{Sm}_{0.875})_{0.52}\text{Sr}_{0.48}\text{MnO}_3$ by the double exchange mechanism.¹³

Recent neutron-scattering study shows that ferromagnetic fluctuations exist above T_{CO} in $\text{Pr}_{1-x}\text{Ca}_x\text{MnO}_3$ ($0.35 \leq x \leq 0.5$).¹⁴ This ferromagnetic correlation is suppressed by the formation of the long-range charge order. It is still unclear that the relationship between the ferromagnetic correlation and the incommensurate lattice modulation. An interpretation is that the short-range charge-ordered regions and the

charge-disordered regions with the ferromagnetic correlation coexist above T_{CO} . High-field x-ray or neutron measurements may provide new insights to clarify this problem, because the ferromagnetic metallic phase is induced by an application of magnetic fields.

We would like to thank K. Torashima and H. Ohtsuka for their assistance in the synchrotron radiation experiment.

This work was partly supported by a Grant-in-Aid for Science Research from the Ministry of Education, Science, Sports and Culture, Japan and by the New Energy and Industrial Technology Development Organization (NEDO) of Japan. The synchrotron radiation experiment was performed at the SPring-8 with the approval of the Japan Synchrotron Radiation Research Institute (JASRI) (Proposal No. 1999B0263-ND-np).

-
- ¹A.J. Millis, *Nature (London)* **392**, 147 (1998).
²S. Shimomura, N. Wakabayashi, H. Kuwahara, and Y. Tokura, *Phys. Rev. Lett.* **83**, 4389 (1999).
³L. Vasiliu-Doloc, S. Rosenkranz, R. Osborn, S.K. Sinha, J.W. Lynn, J. Mesot, O.H. Seeck, G. Preosti, A.J. Fedro, and J.F. Mitchell, *Phys. Rev. Lett.* **83**, 4393 (1999).
⁴Y. Tomioka, A. Asamitsu, H. Kuwahara, Y. Moritomo, and Y. Tokura, *Phys. Rev. B* **53**, R1689 (1996).
⁵Z. Jiráček, S. Krupička, Z. Šimsa, M. Dlouhá, and S. Vratislav, *J. Magn. Magn. Mater.* **53**, 153 (1985).
⁶H. Yoshizawa, H. Kawano, Y. Tomioka, and Y. Tokura, *Phys. Rev. B* **52**, R13 145 (1995); H. Yoshizawa, H. Kawano, Y. Tomioka, and Y. Tokura, *J. Phys. Soc. Jpn.* **65**, 1043 (1996).
⁷D.E. Cox, P.G. Radaelli, M. Marezio, and S-W. Cheong, *Phys. Rev. B* **57**, 3305 (1998).
⁸M.v. Zimmermann, J.P. Hill, Doon Gibbs, M. Blume, D. Casa, B. Keimer, Y. Murakami, Y. Tomioka, and Y. Tokura, *Phys. Rev. Lett.* **83**, 4872 (1999).
⁹N. Wakabayashi, *Phys. Rev. B* **17**, 3875 (1978).
¹⁰P.H. Dederichs, *J. Phys. F: Met. Phys.* **3**, 471 (1973).
¹¹W.L. McMillan, *Phys. Rev. B* **14**, 1496 (1976).
¹²H. Kuwahara, Y. Moritomo, Y. Tomioka, A. Asamitsu, M. Kasai, R. Kumai, and Y. Tokura, *Phys. Rev. B* **56**, 9386 (1997).
¹³C. Zener, *Phys. Rev.* **82**, 403 (1951); P.W. Anderson and H. Hasegawa, *ibid.* **100**, 675 (1955); P.G. de Gennes, *ibid.* **118**, 141 (1960).
¹⁴R. Kajimoto, T. Kakeshita, Y. Oohara, H. Yoshizawa, Y. Tomioka, and Y. Tokura, *Phys. Rev. B* **58**, R11 837 (1998).